Cell Reports

Article

Cortical patterning of morphometric similarity gradient reveals diverged hierarchical organization in sensory-motor cortices

Graphical abstract

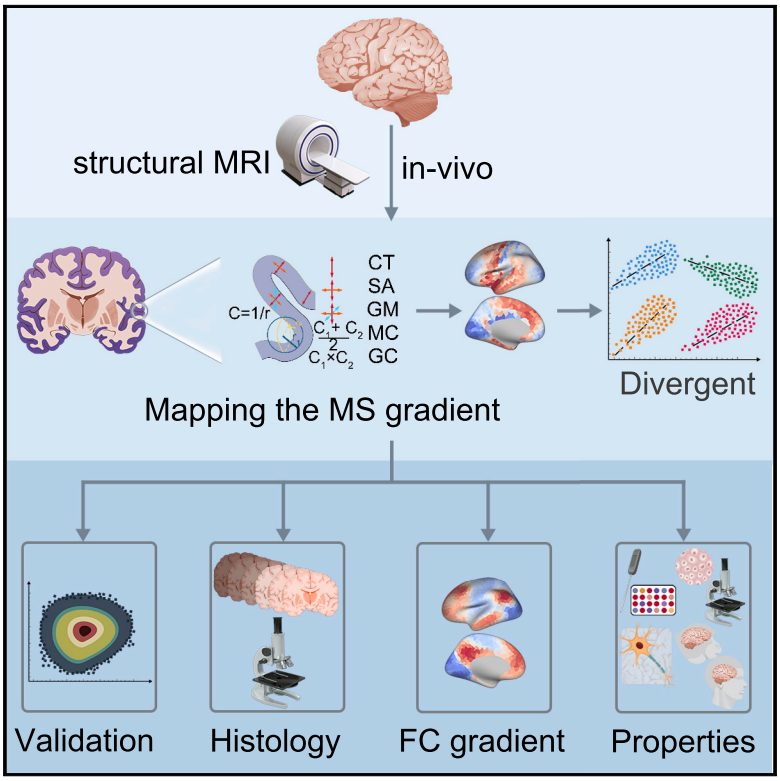

Authors

Siqi Yang, Konrad Wagstyl, Yao Meng, ..., Yun-Shuang Fan, Huafu Chen, Wei Liao

Correspondence

chenhf@uestc.edu.cn (H.C.), weiliao.wl@gmail.com (W.L.)

In brief

Yang et al. investigate the patterning of the cortical morphometric similarity (MS) gradient, which is anchored by sensory and motor cortices and diverges from the functional gradient. The MS gradient also shows similarities to other properties of cortical organization, such as gene expression, cyto-, and myeloarchitecture as well as evolutionary cortical expansion.

Highlights

- Primary motor and sensory areas occupy two extreme ends in the MS gradient
- The MS gradient closely correlates with mesoscale histological layering thickness
- The MS gradient dissociates with the FC gradient in high-level association cortices
- The MS gradient pattern is closely associated with cortical fundamental properties

Yang et al., 2021, Cell Reports *36*, 109582
August 24, 2021
https://doi.org/10.1016/j.celrep.2021.109582

CellPress

Cell Reports

CellPress
OPEN ACCESS

Article

Cortical patterning of morphometric similarity gradient reveals diverged hierarchical organization in sensory-motor cortices

Siqi Yang,[1,2] Konrad Wagstyl,[3] Yao Meng,[1,2] Xiaopeng Zhao,[1,2] Jiao Li,[1,2] Peng Zhong,[1,2] Bing Li,[1,2] Yun-Shuang Fan,[1,2] Huafu Chen,[1,2,*] and Wei Liao[1,2,4,*]

[1]The Clinical Hospital of Chengdu Brain Science Institute, School of Life Science and Technology, University of Electronic Science and Technology of China, Chengdu 611731, P.R. China

[2]MOE Key Lab for Neuroinformation, High-Field Magnetic Resonance Brain Imaging Key Laboratory of Sichuan Province, University of Electronic Science and Technology of China, Chengdu 611731, P.R. China

[3]Wellcome Trust Centre for Neuroimaging, University College London, London, UK

[4]Lead contact

*Correspondence: chenhf@uestc.edu.cn (H.C.), weiliao.wl@gmail.com (W.L.)

https://doi.org/10.1016/j.celrep.2021.109582

SUMMARY

The topological organization of the cerebral cortex provides hierarchical axes, namely gradients, which reveal systematic variations of brain structure and function. However, the hierarchical organization of macroscopic brain morphology and how it constrains cortical function along the organizing axes remains unclear. We map the gradient of cortical morphometric similarity (MS) connectome, combining multiple features conceptualized as a "fingerprint" of an individual's brain. The principal MS gradient is anchored by motor and sensory cortices at two extreme ends, which are reliable and reproducible. Notably, divergences between motor and sensory hierarchies are consistent with the laminar histological thickness gradient but contrary to the canonical functional connectivity (FC) gradient. Moreover, the MS dissociates with FC gradients in the higher-order association cortices. The MS gradient recapitulates fundamental properties of cortical organization, from gene expression and cyto- and myeloarchitecture to evolutionary expansion. Collectively, our findings provide a heuristic hierarchical organization of cortical morphological neuromarkers.

INTRODUCTION

The human cerebral cortex exhibits patterns of areas with structural variations and functional specialization that can be traced to development in ontogeny and evolution (García-Cabezas et al., 2019; Puelles et al., 2019). Cortical areas are differentiated by their gene expressions, cellular compositions, connection features, and positions in cortical hierarchies (Huntenburg et al., 2018). The structure of the cerebral cortex has been examined by Nissl-stained sections in the post-mortem brain via two approaches (García-Cabezas et al., 2020; Sanides and Sas, 1970).

The first, common approach identified cortical areas based on particular cytoarchitectonic features present in some brain areas and absent in others (Amunts et al., 2013; Brodmann, 1909). The second approach described cortical types according to gradual and systematic laminar elaborations. The latter allowed for predictions of laminar patterns of interareal connections based on the structural model (Barbas and Rempel-Clower, 1997; García-Cabezas et al., 2019) and the complexity of sensory representations in each cortical area (Mesulam, 1985, 1998). In visual, somatosensory, and auditory cortices (Grill-Spector and Malach, 2004; Iwamura, 1998; Okada et al., 2010), the primary areas with complex laminar elaboration process particular features of the incoming sensory stimulus, and high-level areas with simple laminar elaboration have increasingly specific and complex responses. In motor-frontal cortices, low-level posterior areas receive signals from high-level frontal, anterior regions, suggesting a rostrocaudal organization for goal-directed behavior and reflecting the gradual variation in structural features, myelination, and cell body density (Badre and D'Esposito, 2009; Thiebaut de Schotten et al., 2017). An essential and fundamental principle in the cortical organization has been proposed to link the gradient of laminar elaboration from limbic areas to primary sensory areas (Sanides and Sas, 1970) with the physiological gradient from primary sensory to multimodal areas (Hubel and Wiesel, 1962), which has been described as a "sensory-fugal" axis (Mesulam, 1985, 1998). Ordering cortical areas along the axis provides a framework to help us understand the relationship among laminar features, cortical connectivity, and the spatial distribution of hierarchical organization.

In addition to histological techniques, magnetic resonance imaging (MRI) facilitates systematic gradient analysis of macrostructural and functional brain measures *in vivo* across the entire human cortex. This entire cortical gradient represents hierarchical organizing axes that describe gradual transitions of structural features and how they constrain cognitive processes

(Margulies et al., 2016; Paquola et al., 2019b). Specifically, the cortex structural gradients derive from a single measurement in various modalities, including MRI thickness covariance (Valk et al., 2020), diffusion MRI tractography (Paquola et al., 2020b; Park et al., 2021b), and cortical-intensity profile covariance (Paquola et al., 2019a, 2019b).These studies have revealed the relationships between cortical structure, cortical connections, and cortical hierarchies in the human brain and have contributed to the understanding of potential mechanisms of neurodevelopment (Burt et al., 2018; Huntenburg et al., 2018; Scholtens et al., 2018; van den Heuvel et al., 2015; van den Heuvel and Yeo, 2017; Wei et al., 2018). However, fiber tractography systematically under-recovers long-distance projections (Dauguet et al., 2007), and structural covariance analysis measures a single morphological feature for a proxy of regional similarities at a group-level (Alexander-Bloch et al., 2013), limiting the ability to characterize morphological gradients at the individual-subject level.

A recently proposed morphometric similarity (MS) connectome, which combines multiple individual morphological features from structural MRIs, elucidates regional morphometric similarities (Seidlitz et al., 2018). The edges of the MS network are highly consistent with regional gene co-expression in the human brain and the axon trajectories of rhesus monkeys (Seidlitz et al., 2018). In addition, the MS connectome predicts a 40% variation in human intelligence (Seidlitz et al., 2018) and provides a alternative neuroimaging phenotype linking brain structural variation to neurogenetic-related gene expressions (Li et al., 2021; Morgan et al., 2019; Seidlitz et al., 2020). However, whether the hierarchical organization of the macroscale MS connectome supports a common ''sensory-fugal'' axis, such as the gradient of laminar elaboration and physiological representations, is not known. Furthermore, it remains to be established how the MS gradient is related to micro-architectural properties directly measured from histology or indirectly inferred from other measurements, such as microarray gene expression and the similarity of microstructure profiles.

In the current study to map the systematic topological organization of cortical morphological features, we constructed the cortical MS by estimating individual brain morphometric features in a cohort of healthy subjects (n = 116); we, then, mapped cortical MS gradients using diffusion map embedding (Vos de Wael et al., 2020), which described gradual transitions at the whole-cortex level and allowed local and long-distance connections to be projected into a common gradient space (Margulies et al., 2016). Next, we assessed the robustness of the MS gradient patterns to variations in the number of morphometric features and spatial resolutions and, then, tested the reproducibility in four independent cohorts. Having characterized the topological pattern of the principal MS gradient, we sought to evaluate the hierarchical organization of the MS gradient. To that end, we calculated cortical geodesic distances from primary areas. We then compared them with the spatial correlations between distance and MS gradients at the whole-cortex level and at four local hierarchies: somatosensory, visual, auditory, and motor hierarchies. Motivated by the finding that the histological thickness gradient diverged in motor and sensory hierarchies (Wagstyl et al., 2020), we combined a six-layered laminar atlas into a multiple linear-regression model to identify the meso-scale histological drivers of the MS gradient. Furthermore, to characterize the structural interpretation of the MS gradient, we analyzed the links between the MS gradient and multiple structural attributes, including brain-specific gene expressions provided by the Allen Human Brain Atlas (Hawrylycz et al., 2012), by cytoarchitectural profiles derived from a post-mortem three-dimensional histological brain sample, by myeloarchitectural features based on the T1-weighted/T2-weighted (T1w/T2w) MRI scans (Paquola et al., 2019b), and by cortical evolutionary expansion (Hill et al., 2010). Moreover, to examine the interplay between the MS gradient and macroscale functional organization, we generated resting-state functional connectome (FC) gradients and directly compared the spatial distribution of the MS/FC gradient correspondence within functional communities and cytoarchitectural classes.

RESULTS

The pattern of the MS gradient

We first divided the entire cortical cortex into 1,533 approximately equally sized subregions (~1 cm^2) based on the Desikan-Killiany (DK) atlas. We extracted five morphometric features, including the gray matter (GM) volume, the surface area (SA), the cortical thickness (CT), the Gaussian curvature (GC), and the mean curvature (MC) for 1,533 regions from structural MRI (T1w) data. To generate individual MS connectomes, we first calculated the regional morphometric features (z-scored) of each pair of regions for each subject. We then evaluated the topological organization of cortical MS connectomes using the diffusion map-embedding technique (Figure 1, see also STAR Methods). In this embedding space, the positions of each parcellation and its neighbors reflected their similarity of morphological profiles. The first component (principal gradient) of the cortical MS accounted for 34% of the variance, with a higher gradient value in the frontal and temporal cortices and a lower value in the occipital and orbital frontal cortices. Rather than considering a single morphometric feature, the MS gradients combined characteristics across multiple morphological measures to estimate intrinsic axes that are more stable as a ''fingerprint'' of an individual's brain. The MS gradients represented an aggregate description of all five features, which reflected variability of every single measure to a varying degree (Figure S1) and was used for exploration in subsequent analysis.

This gradient was anchored at two extreme ends by motor and sensory cortices, with the association cortex in the middle (Figure 2A). Compared with cytoarchitectural classes, the principal gradient described a gradual transition between motor and insula to sensory areas (Figure 2B). Additional gradients explained gradually less-morphological profile variance (Figure S2).

We next assessed the stability and reproducibility of the MS gradients. Using the leave-one-feature-out approach, we verified that the MS gradient is stable for calculating the interareal similarity by calculating the correlation between the full five-feature gradient and the gradient with one measure removed (Figure S3A; see also STAR Methods). To estimate whether the gradients were robust to variations in the numbers of features and spatial resolutions of cortical parcellations, we re-analyzed

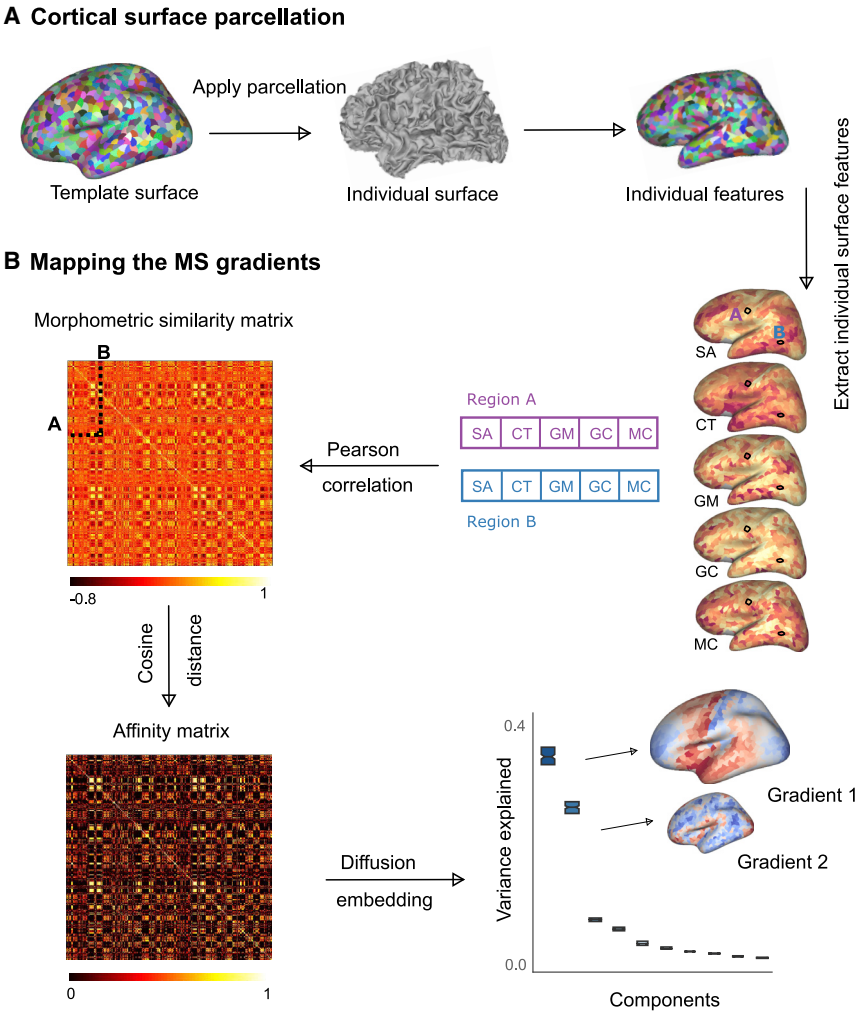

Figure 1. Pipeline for the morphometric similarity (MS) gradients processing

(A) Cortical parcellations were defined using the Desikan-Killiany (DK) atlas with 1,533 sub-regions, which had approximately equal surface areas (~1 cm^2). The template was mapped onto an individual surface to extract the morphological features in each parcellation.

(B) Each region was characterized by a five-feature vector including averaged normalized values of surface area (SA), cortical thickness (CT), gray matter (GM), Gaussian curvature (GC), and mean curvature (MC). The morphometric similarity between each pair of regions was estimated using Pearson's correlation between their feature vector. The matrix was transformed to an affinity matrix, and the diffusion embedding map was used to capture the explained variance.

the MS connectomes derived from seven indices, which included the five features based on T1w data used in the exploratory analyses and another two features derived from diffusion-weight-imaging data, the fractional anisotropy (FA), and an apparent diffusion coefficient (ADC). Regions in the DK-1533 were too small for interpolating values in lower-resolution diffusion tensor imaging (DTI) volumes, so the MS gradient constructed from seven features was mapped onto the DK-308 atlas (the parcel size was approximately 5 cm^2). We noted that the spatial pattern of the MS gradient constructed from seven morphological features was similar to the exploratory findings based on five features (Figure S3B).

In addition, we repeated the gradient analysis using the available cortical features provided by another study (Morgan et al., 2019) and the minimal preprocessing data provided by the Massachusetts General Hospital-University of Southern California (MGH-USC) Human Connectome Project (HCP) dataset (Glasser et al., 2013). When we spatially correlated the MS gradient pattern, significantly positive correlations (all $\rho \geq 0.87$, $p_{spin} < 0.001$) demonstrated excellent reproducibility of the MS gradient (Figure S3C). Taken together, these findings confirmed that the MS gradient was robust to variations in the number of features and individual differences. We used the five-feature MS gradient for the following analysis.

Divergent trends in motor-sensory hierarchies

We found that the primary motor cortex did not occupy a similar position along the MS gradient as sensory areas (Figure 2). To further determine the topological organization of the MS gradient with respect to these primary areas, we first computed the geodesic distance from the primary cortices (Wagstyl et al., 2015) and measured how the morphometric similarity gradients varied with geodesic distance (related to STAR Methods). We assessed the relation between MS gradient and geodesic distance in four local areas, including primary motor, somatosensory, visual, and auditory areas (Figure S4A). In the sensory hierarchies, the MS gradient was positively correlated with the geodesic distance in the somatosensory ($\rho = 0.43$, $p_{spin} < 0.001$), visual ($\rho = 0.80$, $p_{spin} < 0.001$), and auditory cortex ($\rho = 0.20$, $p_{spin} = 0.03$), whereas, in the motor cortex, the MS gradient negatively correlated with distance ($\rho = -0.56$, $p_{spin} < 0.001$) (Figure 3). This divergence in motor-sensory cortices was reproduced in the HCP dataset (Figure S4B; see also STAR Methods).

Motivated by a recent finding that the histological thickness gradient diverged between motor and sensory areas (Wagstyl et al., 2020), we determined whether that histological laminar gradient would provide a meso-scale correlate for the MS gradient. Using the laminar histological atlas (Wagstyl et al., 2020), we linked the MS gradient with mesoscale layering and macroscopic cortical thickness. Furthermore, we estimated whether the cortical layers identifiable by characteristic distributions of different neurons uniformly correlated to the MS gradient. First, we found that the MS gradient positively correlated with the total histological thickness ($\rho = 0.73$,

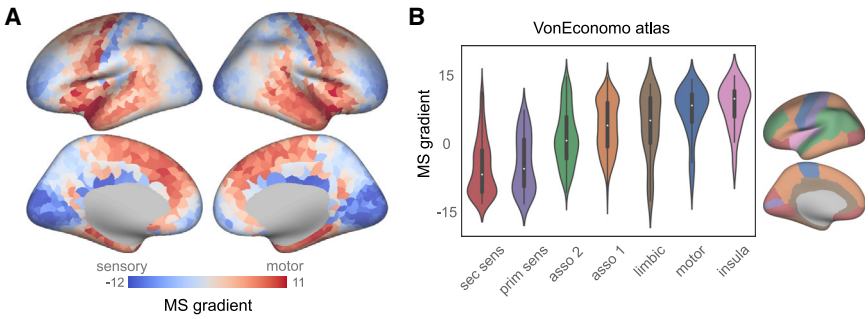

Figure 2. The spatial pattern of the principal MS gradient

(A) The first component in the gradient analysis was mapped onto the DK-1533 atlas.

(B) The average gradient scores within each of the cortical classes of von Economo and Koskinas (1925): sec sens, secondary sensory cortex; prim sens, primary sensory cortex; asso 2, association cortex; asso 1, association cortex; limbic, limbic regions; motor, primary motor; insula, insular cortex.

$p_{spin} < 0.001$) (Figure 4A). Next, we sought to determine each laminar contribution to the MS gradient by constructing a multiple linear-regression model using the *relaimpo* (relative importance of regressors in linear models) R package (Grömping, 2006) (Figure 4B). The model explained 59% of the variance in the MS gradient (Figure 4C; $F_{(6, 1,526)} = 361.4$; $p < 0.05$; adjusted $R^2 = 0.59$), and layers I, III, IV, and V significantly predicted the MS gradient (Figure 4D; Table S1). Notably, layer V had the highest relative importance for the MS gradient in this model, and an inverse contribution was found in layer IV, when compared with other layers. Together, these results suggested that the motor cortex showed a divergence from the sensory cortices in the topological organization of morphometric similarity.

Correspondence of the MS gradient in functional organization

To examine the role of the MS gradient in functional organizations, we compared the spatial correspondence of the cortical morphometric gradients to the functional gradient (Margulies et al., 2016) that was derived from the resting-state functional MRI (rs-fMRI) connectome. To that end, we computed the individual FC matrix, based on the individual DK-1533 template, and then, calculated FC gradients using diffusion map embedding with the same parameters as the MS gradients (related to STAR Methods). Consistent with previous findings (Hong et al., 2019; Margulies et al., 2016; Meng et al., 2021), spatially distributed primary areas, such as visual, somatosensory, and motor cortices, occupied similar positions at one end of the FC gradient. A distributed association cortex occupied the other end (Figure S5A). We noted that the somatosensory and motor areas occupied similar positions along the FC gradient, in contrast to the MS gradient. To study topological features of the morphometric and functional gradients in hierarchical organizations, we first compared both gradients to geodesic distance from primary areas. The FC gradient positively correlated with geodesic distance from primary areas ($\rho = 0.64$, $p_{spin} < 0.001$) (Figure S5C), whereas the MS gradient did not show spatial correspondence. The cortical structure and function may not be organized in the same way across the whole brain (Vázquez-Rodríguez et al., 2019). We also found that the FC gradient positively correlated with the four structural hierarchies ($\rho = 0.75$ for motor cortex, $\rho = 0.67$ for somatosensory cortex, $\rho = 0.44$

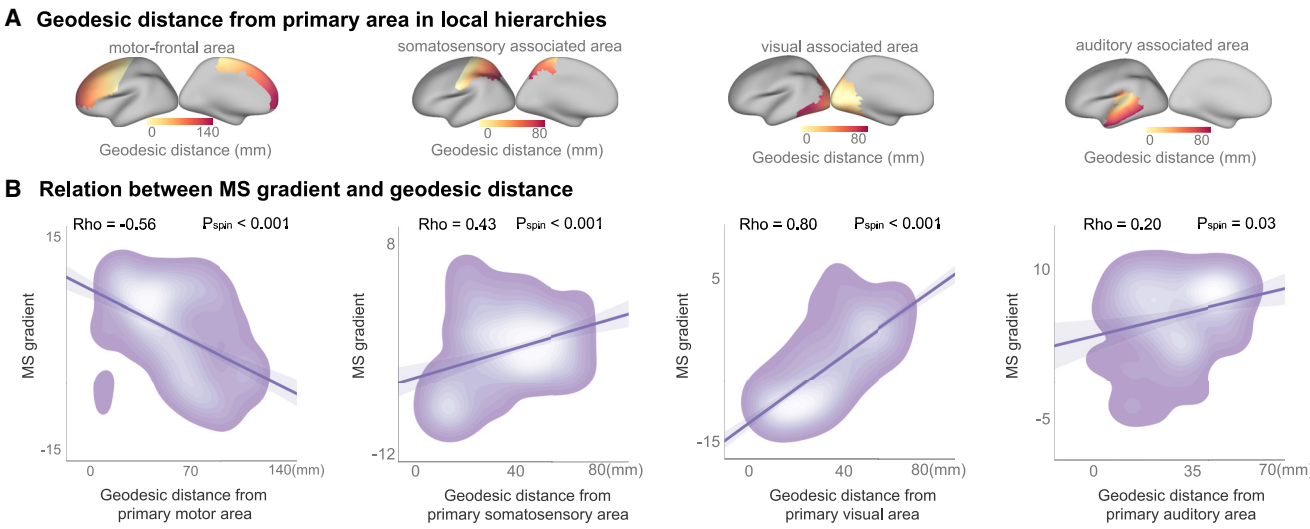

Figure 3. The correlation between the principal MS and distance in local hierarchies

(A) The geodesic distance from the primary areas was used as an index for hierarchical levels in four local hierarchies.

(B) In a motor hierarchy, the principal MS gradient negatively correlated with the geodesic distance ($\rho = -0.56$, $p_{spin} < 0.001$), whereas in the sensory hierarchies ($\rho = 0.43$ for somatosensory cortices, $\rho = 0.80$ for visual cortices, $\rho = 0.20$ for auditory cortices, all $p_{spin} < 0.05$), the principal MS positively correlated with the geodesic distance.

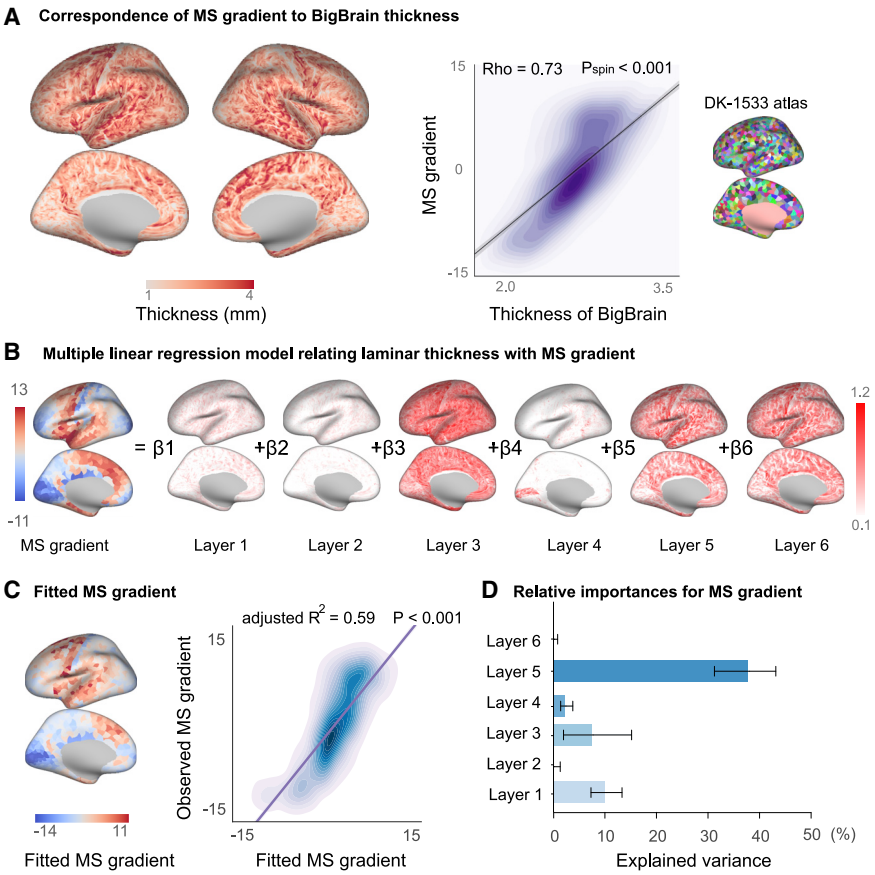

Figure 4. Associations between the principal MS gradient and the laminar histological thickness

(A) The principal MS gradient was positively correlated with the total histological thickness (ρ = 0.73, $p_{spin} < 0.001$).

(B) A multiple linear-regression model was used to determine the relationship between the MS gradient and the laminar histological atlas.

(C) The predicted MS gradient values and a plot of the predicted versus observed gradients (adjusted $R^2 = 0.59$, $p < 0.05$).

(D) The relative importance of each laminar regression contributing to the multiple linear regression model was assessed using the *relaimpo* R package. Error bar, 95% bootstrap confidence intervals.

for visual cortex, and $\rho = 0.85$ for auditory cortex, all $p_{spin} < 0.001$) (Figure S5D), whereas the MS gradient showed an inverse correlation in motor-frontal cortices. We then directly calculated the differences in the MS and FC gradients by comparing region ranks across the entire cortex and within functional communities/cytoarchitectural classes. Cortex-wise region-rank comparisons revealed shifts in motor areas to the MS gradient and a converse shift in high-level association cortices to the FC gradient (Figure 5A). Although some functional networks were distributed across the morphometric gradient, they were located at a similar level in the functional gradient, such as somatosensory and motor areas in one end and the default mode fronto-parietal networks in another end. When comparing node ranks within functional communities, we found a dissociation of the MS gradient from function in sensorimotor areas and a converse dissociation of FC gradient from morphology in the frontoparietal and default mode network (Figure 5B). Consistent findings were found in comparisons of cytoarchitectural classes, which showed that differences of two gradients were exhibited in the primary motor and association areas (Figure 5C). The statistical results of a paired t test across individuals in gradients between structure and function are listed in Table S2. Conducting a meta-analysis using the NeuroSynth database (Yarkoni et al., 2011), we observed a functional variation of the MS gradient at one end, related to "visuospatial" and "reading," with the other end related to "reward" and "emotion" (Figure S6).

Relation to the hierarchical organization of microstructures

Having examined the hierarchical organization of the MS gradient, we next sought to understand its relationship to fundamental properties of brain organization (related to STAR Methods). Morphometric similarity measured by an MRI is a well-known indication of histological similarity (Barbas and Rempel-Clower, 1997; Seidlitz et al., 2018; Wei et al., 2018). We next compared the MS gradient with multiple microstructural profiles, including gene expression, cell density, and myelin content, to reveal the systematic spatial relationships of cortical properties at different scales (Figures 6A–6C). At the microscale and mesoscale levels, parcel-wise analyses showed strong spatial correlations of the MS gradient with the first component of gene expression (ρ = –0.73, $p_{spin} < 0.001$), cytoarchitectural similarity profile (ρ = 0.47, $p_{spin} < 0.001$), as well as a moderate correlation with myeloarchitectural similarity (ρ = 0.41, p_{spin} = 0.02).

Furthermore, cortical expansion had nonuniform distributions, reflecting regional morphological differences in evolution. The high expansion was related to the dorsal frontal, lateral temporal, and lateral parietal cortices, and low expansion to the occipital and medial temporal cortices. To understand how evolutionary properties constrained the interregional morphological similarity, we also compared the MS gradient with maps of evolutionary cortical expansions. We also observed a positive spatial correlation between the MS gradient and cortical expansion (ρ = 0.35, p_{spin} = 0.03) (Figure 6D). Thus, the topological organization of cortical morphology varied along the microscale underpins and was constrained by the cortical hierarchies of evolutionary expansion.

DISCUSSION

Cortical regions along the embedding axis capture the gradual variation in morphometric similarity, reflecting their gene

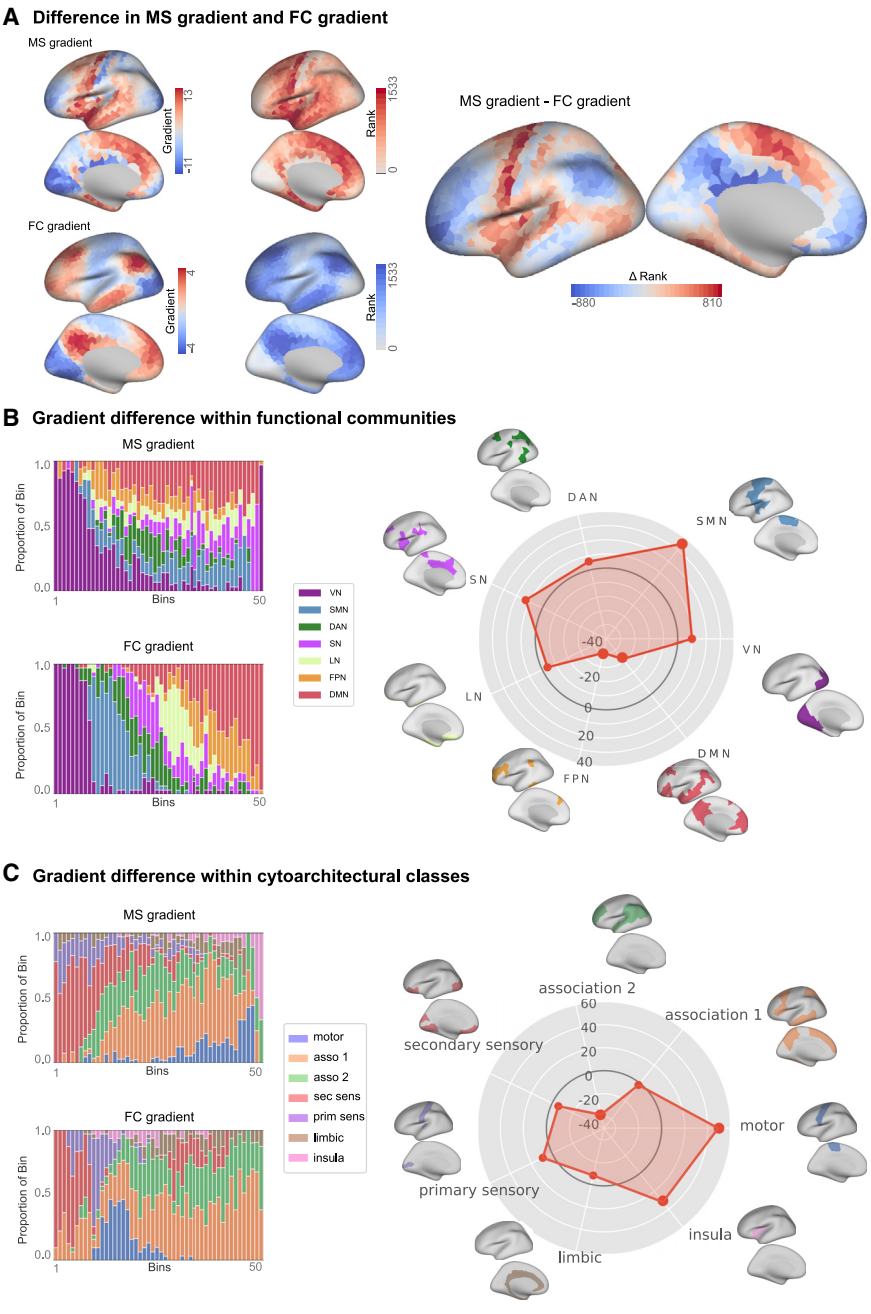

Figure 5. Correspondence of the principal MS gradient to the functional organization

(A) Node rank difference between the principal MS gradient and the FC gradient.

(B and C) The principal MS gradient and FC gradient were discretized into 50 equally sized bins, and stacked bar plots depict the proportion of each bin accounted for within each functional community (B) and cytoarchitecture class (C). A radar plot shows the difference of mean node ranks corresponding to the community/class between the two gradients. VN, visual network; SMN, somato-motor network; DAN, dorsal attention network; VAN, ventral attention network; LN, limbic network; FPN, fronto-parietal network; DMN, default mode network.

expression, cellular density, and myelin content (García-Cabezas et al., 2020; Huntenburg et al., 2018). In this study, leveraging the diffusion map embedding technology, we investigated the low-dimension representations (gradients) of cortical morphometric similarity. The MS gradients showed robust stability in the variation of the numbers of morphological features and spatial resolutions of the cortical parcellations and reproducibility in independent datasets. The principal gradient showed diverged patterns in sensory and motor areas, placing them at a different level in cytoarchitectural classes. Specifically, the spatial layout of cortical areas across visual, somatosensory, and auditory hierarchies from primary sensory areas to high-level areas paralleled the distribution of those areas across the MS gradient, showing a transition of increasing MS gradient; however, the motor-frontal cortices showed a decreasing MS gradient from the primary motor to high-level cortices. Furthermore, we also observed a dissociation between the morphometric and functional gradients in motor and default mode networks, indicating distinctive structural complexity in motor areas, as well as functional flexibility in high-level association areas. Taken together, the hierarchical organization of the macroscopic morphometric profiles provided insight into understanding cortical structure-function correspondence.

The morphometric similarity connectome has a complex topology (Seidlitz et al., 2018), and gradient approaches have, instead, found the principal axes of variance in this connectome through manifold-learning techniques, which offer a valuable perspective to bridge low-dimensional representations of cortical organization and human cognition (Margulies et al., 2016). Previous studies have characterized the topological properties of the MS network, including the degree distribution, the small-worldness, the community structure, and a rich club (Galdi et al., 2020; Li et al., 2017, 2021; Morgan et al., 2019; Seidlitz et al., 2018, 2020). Importantly, the network phenotype of the morphometric similarity changes was associated with disease-related alterations of specific genes, providing a biological combination analysis of neuroimaging and transcriptional data (Morgan et al., 2019). Directly analyzing the embedded spaces derived from the MS connectome, the MS gradient, revealed that gradients could serve as cortical coordinates describing the relationship between interconnected areas. Recently, similar algorithms have

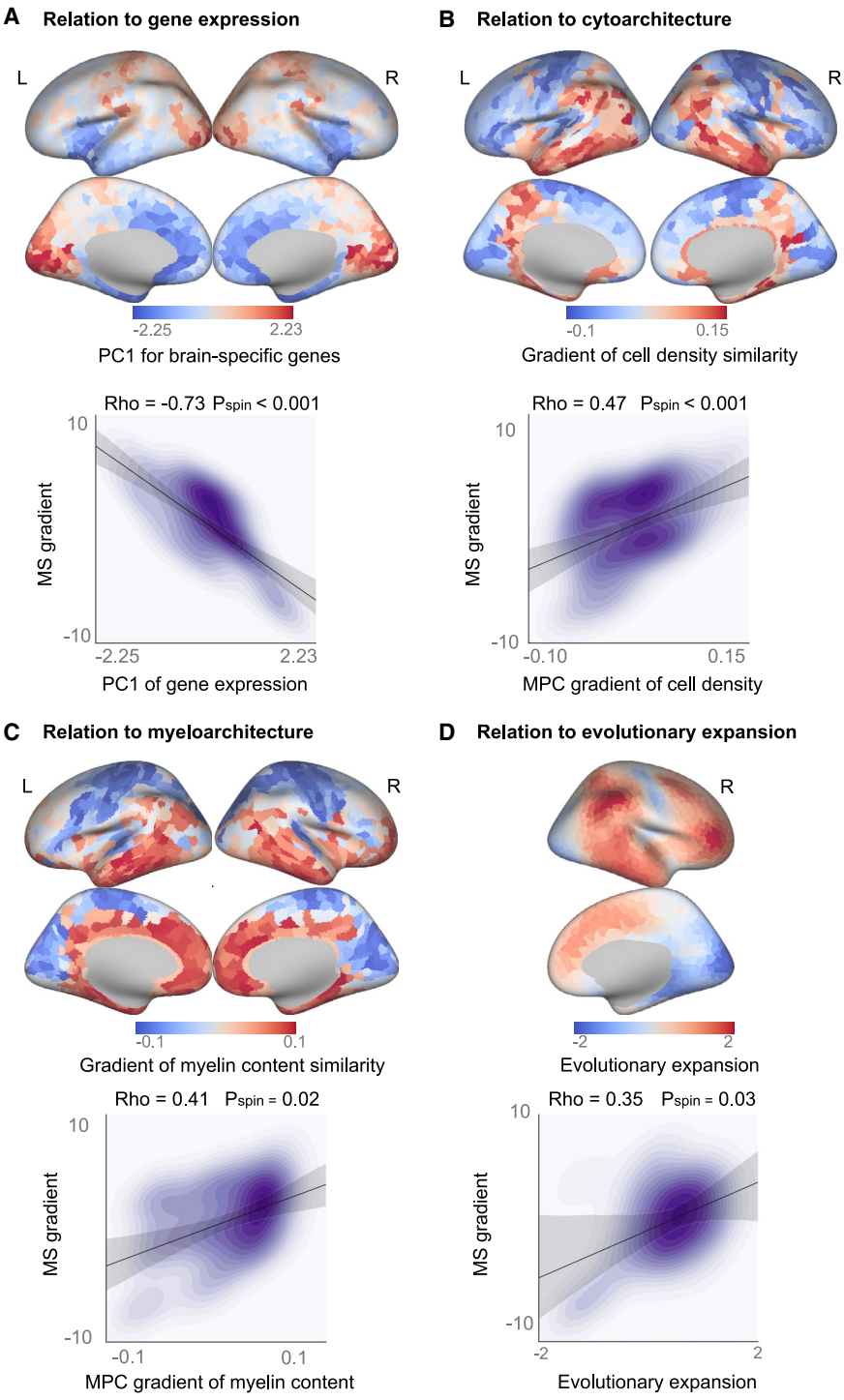

Figure 6. Relation to cortical microstructure and expansion

The principal MS gradient correlated with the principal component of brain-specific gene expression (ρ = –0.73, p_{spin} < 0.001) (A), interregional similarity in cell density (ρ = 0.47, p_{spin} < 0.001) (B) and myelin content (ρ = 0.41, p_{spin} = 0.02) (C), as well as the evolutionary expansion (ρ = 0.35, p_{spin} = 0.03) (D).

been used to identify structural gradients constructed using various approaches. For example, the main gradients of interregional cortical-thickness correlations supported the important role of genetic influence in the macroscale organization of the human cortex (Valk et al., 2020). Other studies provided low-dimensional representations of diffusion MRI tractography, which suggested distinct structural constraints on functional dynamics between low-level regions and the transmodal cortex (Park et al., 2021b). They constructed the cortical wiring to examine macroscopic changes in structural connectivity in autism spectrum disorders (Park et al., 2021a). Many studies have shown the spatial layout of cortical hierarchies in multiple gradients of different cortical structure along the "sensory-fugal" axis, such as cytoarchitectural and myeloarchitectural profiles (Paquola et al., 2019b), excitatory/inhibitory receptor ratios (Goulas et al., 2021), and anatomical centrality of diffusion tractography (Zhang et al., 2020). Our study added to a growing understanding of the relationship between cortical structures, cortical connections, and cortical hierarchies in humans, by combining multiple structural features that were not previously studied.

In contrast to the "canonical" functional gradient, the primary motor did not localize to the same position in the MS gradient as in the sensory areas. This interesting finding may be caused by distinctive histological properties in the motor cortex. Unlike sensory areas, the primary motor area has a lower neuronal density (Rockel et al., 1980), lower neurotransmitter receptor density (Zilles and Palomero-Gallagher, 2017), greater thickness (Wagstyl et al., 2020), and distinct laminar characteristics (von Economo and Koskinas, 1925). Significantly, we found that these divergent characteristics of the MS gradient were consistent with patterns of histological cortical thickness. We found positive contributions in layers I, III, and V, with an inverse contribution in layer IV. Among the six layers, this correspondence was strongest in pyramidal neuron layers III and V and could be driven by changes in pyramidal neuronal arborizations. Layer IV consisted mostly of stellate cells and a smaller portion of the pyramidal cells. Granular cells, as the dominant cellular component, contributed to the formation of specific sensory cortical areas. This layer was the main target

of cortical-afferent connections, and for that reason, it was especially developed within the sensory areas. Unlike layers III, V, and VI, the average thickness of layer IV was relatively thin, but it was significantly thicker in the visual area than it was in the other cortical areas. By volume, the cortex is 90% neuropil, to which dendrites and synapses are major contributors (Braitenberg and Schüz, 1991). Thus, changes in the size of neuronal arbors could directly affect our *in vivo* morphometric measures (volume, surface area, and curvature) through changes in cortical surface expansion. Furthermore, the genetic topography of the cortex is known to follow a similar hierarchical topography (Zilles and Amunts, 2012), which is likely to underpin the gradient pattern of cortical morphological features. We noted that the insula cortex occupied one extreme in the MS gradient, similar to the motor cortex. This may be due to the heterogeneous structure in the insula characterized by less-differentiated cortical layers (Nieuwenhuys, 2012), yet differ from the sensory cortices with clear laminar differentiation. However, the insula is also a highly folded and buried cortex, where precise identification of the inner and outer contours is difficult to obtain using MRI. These factors often lead to over-estimated MRI thickness values for insular and peri-insular regions (Wagstyl et al., 2020). We also noted a distinct transition of the MS gradient within the limbic cortex and a relatively wide distribution of data in the violin plot in this cytoarchitectural class (Figure 2). Convergent evidence has suggested that a sequential progression of cortical architectonic differentiation arises from the mesocortical limbic area (Goulas et al., 2019; Paquola et al., 2020a; Puelles et al., 2019; Sanides, 1969; Valk et al., 2020), forming transition zones between the isocortex and allocortex and resulting in a ''sensory-fugal'' organization.

We observed common and specific hierarchical organization between the structural and functional gradients. Geodesic distance from the primary areas was used as an alternative index for the hierarchical level (Wagstyl et al., 2015), and increased distance reflected more-specialized functions. In sensory hierarchies, regions are situated a long distance from the primary sensory areas, along with upward morphometric and functional gradients. Unlike the principal functional gradient, the motor-frontal cortices showed an inverse transition compared with sensory hierarchies in the MS gradient. Histologically, the trends of variation in the MS gradient from the motor to frontal areas were consistent with changes in cellular density and cortical thickness, which diverged from the pattern in other cortical regions (Collins et al., 2010; Wagstyl et al., 2020). Functionally, the motor cortex was located on the frontal lobe, which had a more-variable structure during the development and had a crucial role in cognitive controls.

Moreover, motor processing and sensory processing possessed the reverse direction of information flow. The motor areas received signals from the anterior frontal cortices, which supported a hierarchy of action controls along the rostrocaudal axis (Badre and D'Esposito, 2009), whereas, in sensory-processing hierarchies, primary cortices responded to the most basic stimuli, and then, the higher areas selectively responded to certain types of sensory stimuli (Grill-Spector and Malach, 2004; Okada et al., 2010). In addition to these distributed, local hierarchies, the comparison between morphometric and functional gradients at the whole-cortex scale suggested a flexible functional role in cortices of high-level association. A medial position of the association cortices in the MS axis showed dissimilarity to both extreme ends. It made it different than primary areas, which had distinctive cytoarchitectonic and functional grounds. This morphometric axis resembled a natural axis of excitatory/inhibitory receptor ratios, which revealed a progressive transition from the sensory to the association and primary motor areas (Goulas et al., 2021).

Limitations

This study had several limitations. First, different spatial scales determined by cortical parcellations affected gradient identification and analysis. Finer spatial resolution contributed to more-marked transitions in the overall shape of the gradients. However, the high spatial resolution reduced the registration results from individual surface space into the volume space. We, therefore, used five morphometric features (not including the diffusion index) to construct the MS gradient during exploratory analyses to capture the stability gradient pattern. Although we demonstrated consistency between the MS gradient derived from different cortical features, the balance of the spatial scale and the regional features is still worth considering. Second, the cerebral cortex has a laminar structure, and each layer exhibits different anatomical properties; the resolution of the MRI was not sufficient to identify finer laminar-scale morphological features. Recent studies of layer-specific interarea variations extended our understanding of the structure and function in the human cortex (García-Cabezas et al., 2020; Goulas et al., 2021; Nieuwenhuys and Broere, 2020; Paquola et al., 2019b). We can also determine the relationship between MS gradients and more layer-specific properties, such as gene expression and transmitter receptors, etc. In the present study, we mainly focused on the principal MS gradient, so extended representations could be meaningful to complete the framework for describing the cortical hierarchical organization.

Conclusion

The MS gradient describing the interregional morphological similarity is anchored at the two extreme ends by motor and sensory cortices. Moreover, with increased hierarchical distance from the primary cortices, the association cortices, situated between the two ends in the MS gradient, conduced to their flexible functions. Notably, the morphological gradient diverged in the motor-frontal and sensory cortices, identifying novel nuances in the relationships between cortical structure and function. Together, our findings provide insight into understanding the coordination of structure and function in a hierarchical organization.

STAR★METHODS

Detailed methods are provided in the online version of this paper and include the following:

- KEY RESOURCES TABLE
- RESOURCE AVAILABILITY
  - Lead contact
  - Materials availability

SUPPLEMENTAL INFORMATION

Supplemental information can be found online at https://doi.org/10.1016/j.celrep.2021.109582.

ACKNOWLEDGMENTS

We are grateful to all the participants in this study. We thank International Science Editing (https://www.internationalscienceediting.com) for editing this manuscript. This study was funded by the Key Project of Research and Development of Ministry of Science and Technology (2018AAA0100705), the National Natural Science Foundation of China (61871077, 62036003, and U1808204), and the Excellent Youth Foundation of the Sichuan Scientific Committee (2020JDJQ0016).

AUTHOR CONTRIBUTIONS

Conceptualization, supervision, project administration, and funding acquisition, W.L. and H.C.; formal analysis, Y.M.; methodology, S.Y., X.Z., P.Z., and B.L.; resources, J.L.; software: Y.M. and S.Y.; visualization, S.Y. and Y.-S.F.; validation, S.Y. and Y.M.; writing – original draft, S.Y. and K.W.; writing – review & editing, S.Y., K.W., and W.L.

DECLARATION OF INTERESTS

The authors declare no competing interests.

INCLUSION AND DIVERSITY

We worked to ensure gender balance in the recruitment of human subjects. We worked to ensure ethnic or other types of diversity in the recruitment of human subjects. We worked to ensure that the study questionnaires were prepared in an inclusive way. While citing references scientifically relevant for this work, we also actively worked to promote gender balance in our reference list.

Received: December 18, 2020
Revised: May 28, 2021
Accepted: July 30, 2021
Published: August 24, 2021

REFERENCES

Alexander-Bloch, A., Raznahan, A., Bullmore, E., and Giedd, J. (2013). The convergence of maturational change and structural covariance in human cortical networks. J. Neurosci. *33*, 2889–2899.

Alexander-Bloch, A.F., Shou, H., Liu, S., Satterthwaite, T.D., Glahn, D.C., Shinohara, R.T., Vandekar, S.N., and Raznahan, A. (2018). On testing for spatial correspondence between maps of human brain structure and function. Neuroimage *178*, 540–551.

Amunts, K., Lepage, C., Borgeat, L., Mohlberg, H., Dickscheid, T., Rousseau, M.E., Bludau, S., Bazin, P.L., Lewis, L.B., Oros-Peusquens, A.M., et al. (2013). BigBrain: an ultrahigh-resolution 3D human brain model. Science *340*, 1472–1475.

Arnatkeviciute, A., Fulcher, B.D., and Fornito, A. (2019). A practical guide to linking brain-wide gene expression and neuroimaging data. Neuroimage *189*, 353–367.

Badre, D., and D'Esposito, M. (2009). Is the rostro-caudal axis of the frontal lobe hierarchical? Nat. Rev. Neurosci. *10*, 659–669.

Barbas, H., and Rempel-Clower, N. (1997). Cortical structure predicts the pattern of corticocortical connections. Cereb. Cortex *7*, 635–646.

Braitenberg, V., and Schüz, A. (1991). Anatomy of the Cortex: Statistics and geometry (Springer-Verlag Publishing).

Brodmann, K. (1909). Brodmann's Localisation in the Cerebral Cortex [Translated from German by Laurence J. Garey] (Imperial College Press).

Burt, J.B., Demirtaş, M., Eckner, W.J., Navejar, N.M., Ji, J.L., Martin, W.J., Bernacchia, A., Anticevic, A., and Murray, J.D. (2018). Hierarchy of transcriptomic specialization across human cortex captured by structural neuroimaging topography. Nat. Neurosci. *21*, 1251–1259.

Collins, C.E., Airey, D.C., Young, N.A., Leitch, D.B., and Kaas, J.H. (2010). Neuron densities vary across and within cortical areas in primates. Proc. Natl. Acad. Sci. USA *107*, 15927–15932.

Dauguet, J., Peled, S., Berezovskii, V., Delzescaux, T., Warfield, S.K., Born, R., and Westin, C.F. (2007). Comparison of fiber tracts derived from in-vivo DTI tractography with 3D histological neural tract tracer reconstruction on a macaque brain. Neuroimage *37*, 530–538.

Desikan, R.S., Ségonne, F., Fischl, B., Quinn, B.T., Dickerson, B.C., Blacker, D., Buckner, R.L., Dale, A.M., Maguire, R.P., Hyman, B.T., et al. (2006). An automated labeling system for subdividing the human cerebral cortex on MRI scans into gyral based regions of interest. Neuroimage *31*, 968–980.

Destrieux, C., Fischl, B., Dale, A., and Halgren, E. (2010). Automatic parcellation of human cortical gyri and sulci using standard anatomical nomenclature. Neuroimage *53*, 1–15.

Fischl, B. (2012). FreeSurfer. Neuroimage *62*, 774–781.

Fischl, B., Liu, A., and Dale, A.M. (2001). Automated manifold surgery: constructing geometrically accurate and topologically correct models of the human cerebral cortex. IEEE Trans. Med. Imaging *20*, 70–80.

Fischl, B., van der Kouwe, A., Destrieux, C., Halgren, E., Ségonne, F., Salat, D.H., Busa, E., Seidman, L.J., Goldstein, J., Kennedy, D., et al. (2004). Automatically parcellating the human cerebral cortex. Cereb. Cortex *14*, 11–22.

Galdi, P., Blesa, M., Stoye, D.Q., Sullivan, G., Lamb, G.J., Quigley, A.J., Thrippleton, M.J., Bastin, M.E., and Boardman, J.P. (2020). Neonatal morphometric similarity mapping for predicting brain age and characterizing neuroanatomic variation associated with preterm birth. Neuroimage Clin. *25*, 102195.

García-Cabezas, M.A., Zikopoulos, B., and Barbas, H. (2019). The structural model: a theory linking connections, plasticity, pathology, development and evolution of the cerebral cortex. Brain Struct. Funct. *224*, 985–1008.

García-Cabezas, M.A., Hacker, J.L., and Zikopoulos, B. (2020). A protocol for cortical type analysis of the human neocortex applied on histological samples, the atlas of Von Economo and Koskinas, and magnetic resonance imaging. Front. Neuroanat. *14*, 576015.

Glasser, M.F., Sotiropoulos, S.N., Wilson, J.A., Coalson, T.S., Fischl, B., Andersson, J.L., Xu, J., Jbabdi, S., Webster, M., Polimeni, J.R., et al.; WU-Minn HCP Consortium (2013). The minimal preprocessing pipelines for the Human Connectome Project. Neuroimage *80*, 105–124.

Gordon, E.M., Laumann, T.O., Adeyemo, B., Huckins, J.F., Kelley, W.M., and Petersen, S.E. (2016). Generation and evaluation of a cortical area parcellation from resting-state correlations. Cereb. Cortex *26*, 288–303.

Goulas, A., Margulies, D.S., Bezgin, G., and Hilgetag, C.C. (2019). The architecture of mammalian cortical connectomes in light of the theory of the dual origin of the cerebral cortex. Cortex *118*, 244–261.

Goulas, A., Changeux, J.P., Wagstyl, K., Amunts, K., Palomero-Gallagher, N., and Hilgetag, C.C. (2021). The natural axis of transmitter receptor distribution in the human cerebral cortex. Proc. Natl. Acad. Sci. USA *118*, e2020574118.

Greve, D.N., and Fischl, B. (2009). Accurate and robust brain image alignment using boundary-based registration. Neuroimage *48*, 63–72.

Grill-Spector, K., and Malach, R. (2004). The human visual cortex. Annu. Rev. Neurosci. *27*, 649–677.

Grömping, U. (2006). Relative importance for linear regression in R: the package relaimpo. J. Stat. Softw. *17*, 1–27.

Hawrylycz, M.J., Lein, E.S., Guillozet-Bongaarts, A.L., Shen, E.H., Ng, L., Miller, J.A., van de Lagemaat, L.N., Smith, K.A., Ebbert, A., Riley, Z.L., et al. (2012). An anatomically comprehensive atlas of the adult human brain transcriptome. Nature *489*, 391–399.

Hill, J., Inder, T., Neil, J., Dierker, D., Harwell, J., and Van Essen, D. (2010). Similar patterns of cortical expansion during human development and evolution. Proc. Natl. Acad. Sci. USA *107*, 13135–13140.

Hodge, M.R., Horton, W., Brown, T., Herrick, R., Olsen, T., Hileman, M.E., McKay, M., Archie, K.A., Cler, E., Harms, M.P., et al. (2016). ConnectomeDB—sharing human brain connectivity data. Neuroimage *124* (*Pt B*), 1102–1107.

Hong, S.J., Vos de Wael, R., Bethlehem, R.A.I., Lariviere, S., Paquola, C., Valk, S.L., Milham, M.P., Di Martino, A., Margulies, D.S., Smallwood, J., and Bernhardt, B.C. (2019). Atypical functional connectome hierarchy in autism. Nat. Commun. *10*, 1022.

Hubel, D.H., and Wiesel, T.N. (1962). Receptive fields, binocular interaction and functional architecture in the cat's visual cortex. J. Physiol. *160*, 106–154.

Huntenburg, J.M., Bazin, P.L., and Margulies, D.S. (2018). Large-scale gradients in human cortical organization. Trends Cogn. Sci. *22*, 21–31.

Iwamura, Y. (1998). Hierarchical somatosensory processing. Curr. Opin. Neurobiol. *8*, 522–528.

Jenkinson, M., Bannister, P., Brady, M., and Smith, S. (2002). Improved optimization for the robust and accurate linear registration and motion correction of brain images. Neuroimage *17*, 825–841.

Jenkinson, M., Beckmann, C.F., Behrens, T.E., Woolrich, M.W., and Smith, S.M. (2012). Fsl. Neuroimage *62*, 782–790.

Kong, R., Li, J., Orban, C., Sabuncu, M.R., Liu, H., Schaefer, A., Sun, N., Zuo, X.N., Holmes, A.J., Eickhoff, S.B., and Yeo, B.T.T. (2019). Spatial topography of individual-specific cortical networks predicts human cognition, personality, and emotion. Cereb. Cortex *29*, 2533–2551.

Li, W., Yang, C., Shi, F., Wu, S., Wang, Q., Nie, Y., and Zhang, X. (2017). Construction of individual morphological brain networks with multiple morphometric features. Front. Neuroanat. *11*, 34.

Li, J., Seidlitz, J., Suckling, J., Fan, F., Ji, G.J., Meng, Y., Yang, S., Wang, K., Qiu, J., Chen, H., and Liao, W. (2021). Cortical structural differences in major depressive disorder correlate with cell type-specific transcriptional signatures. Nat. Commun. *12*, 1647.

Margulies, D.S., Ghosh, S.S., Goulas, A., Falkiewicz, M., Huntenburg, J.M., Langs, G., Bezgin, G., Eickhoff, S.B., Castellanos, F.X., Petrides, M., et al. (2016). Situating the default-mode network along a principal gradient of macroscale cortical organization. Proc. Natl. Acad. Sci. USA *113*, 12574–12579.

Markello, R.D., Arnatkevičiūtė, A., Poline, J.-B., Fulcher, B.D., Fornito, A., and Misic, B. (2021). Standardizing workflows in imaging transcriptomics with the abagen toolbox. bioRxiv. https://doi.org/10.1101/2021.07.08.451635.

Meng, Y., Yang, S., Chen, H., Li, J., Xu, Q., Zhang, Q., Lu, G., Zhang, Z., and Liao, W. (2021). Systematically disrupted functional gradient of the cortical connectome in generalized epilepsy: Initial discovery and independent sample replication. Neuroimage *230*, 117831.

Mesulam, M.M. (1985). Patterns in behavioral neuroanatomy: association areas, the limbic system, and hemispheric specialization. In Principles of Behavioral Neurology (F.A. Davis), pp. 1–70.

Mesulam, M.M. (1998). From sensation to cognition. Brain *121*, 1013–1052.

Morgan, S.E., Seidlitz, J., Whitaker, K.J., Romero-Garcia, R., Clifton, N.E., Scarpazza, C., van Amelsvoort, T., Marcelis, M., van Os, J., Donohoe, G., et al. (2019). Cortical patterning of abnormal morphometric similarity in psychosis is associated with brain expression of schizophrenia-related genes. Proc. Natl. Acad. Sci. USA *116*, 9604–9609.

Nieuwenhuys, R. (2012). The insular cortex: a review. In Brain Research, Chapter 7, M.A. Hofman and D. Falk, eds. (Elsevier), pp. 123–163.

Nieuwenhuys, R., and Broere, C.A.J. (2020). A detailed comparison of the cytoarchitectonic and myeloarchitectonic maps of the human neocortex produced by the Vogt-Vogt school. Brain Struct. Funct. *225*, 2717–2733.

Okada, K., Rong, F., Venezia, J., Matchin, W., Hsieh, I.H., Saberi, K., Serences, J.T., and Hickok, G. (2010). Hierarchical organization of human auditory cortex: evidence from acoustic invariance in the response to intelligible speech. Cereb. Cortex *20*, 2486–2495.

Oligschläger, S., Huntenburg, J.M., Golchert, J., Lauckner, M.E., Bonnen, T., and Margulies, D.S. (2017). Gradients of connectivity distance are anchored in primary cortex. Brain Struct. Funct. *222*, 2173–2182.

Paquola, C., Bethlehem, R.A., Seidlitz, J., Wagstyl, K., Romero-Garcia, R., Whitaker, K.J., Vos de Wael, R., Williams, G.B., Vértes, P.E., Margulies, D.S., et al.; NSPN Consortium (2019a). Shifts in myeloarchitecture characterise adolescent development of cortical gradients. eLife *8*, e50482.

Paquola, C., Vos De Wael, R., Wagstyl, K., Bethlehem, R.A.I., Hong, S.J., Seidlitz, J., Bullmore, E.T., Evans, A.C., Misic, B., Margulies, D.S., et al. (2019b). Microstructural and functional gradients are increasingly dissociated in transmodal cortices. PLoS Biol. *17*, e3000284.

Paquola, C., Benkarim, O., DeKraker, J., Larivière, S., Frässle, S., Royer, J., Tavakol, S., Valk, S., Bernasconi, A., Bernasconi, N., et al. (2020a). Convergence of cortical types and functional motifs in the human mesiotemporal lobe. eLife *9*, e60673.

Paquola, C., Seidlitz, J., Benkarim, O., Royer, J., Klimes, P., Bethlehem, R.A.I., Larivière, S., Vos de Wael, R., Rodríguez-Cruces, R., Hall, J.A., et al. (2020b). A multi-scale cortical wiring space links cellular architecture and functional dynamics in the human brain. PLoS Biol. *18*, e3000979.

Park, B.Y., Hong, S.J., Valk, S.L., Paquola, C., Benkarim, O., Bethlehem, R.A.I., Di Martino, A., Milham, M.P., Gozzi, A., Yeo, B.T.T., et al. (2021a). Differences in subcortico-cortical interactions identified from connectome and microcircuit models in autism. Nat. Commun. *12*, 2225.

Park, B.Y., Vos de Wael, R., Paquola, C., Larivière, S., Benkarim, O., Royer, J., Tavakol, S., Cruces, R.R., Li, Q., Valk, S.L., et al. (2021b). Signal diffusion along connectome gradients and inter-hub routing differentially contribute to dynamic human brain function. Neuroimage *224*, 117429.

Puelles, L., Alonso, A., García-Calero, E., and Martínez-de-la-Torre, M. (2019). Concentric ring topology of mammalian cortical sectors and relevance for patterning studies. J. Comp. Neurol. *527*, 1731–1752.

Rockel, A.J., Hiorns, R.W., and Powell, T.P. (1980). The basic uniformity in structure of the neocortex. Brain *103*, 221–244.

Romero-Garcia, R., Atienza, M., Clemmensen, L.H., and Cantero, J.L. (2012). Effects of network resolution on topological properties of human neocortex. Neuroimage *59*, 3522–3532.

Sanides, F. (1969). Comparative architectonics of the neocortex of mammals and their evolutionary interpretation. Ann. N Y Acad. Sci. *167*, 404–423.

Sanides, F., and Sas, E. (1970). Persistence of horizontal cells of the Cajal foetal type and of the subpial granular layer in parts of the mammalian paleocortex. Z. Mikrosk. Anat. Forsch. *82*, 570–588.

Scholtens, L.H., de Reus, M.A., de Lange, S.C., Schmidt, R., and van den Heuvel, M.P. (2018). An MRI: von Economo-Koskinas atlas. Neuroimage *170*, 249–256.

Ségonne, F., Pacheco, J., and Fischl, B. (2007). Geometrically accurate topology-correction of cortical surfaces using nonseparating loops. IEEE Trans. Med. Imaging *26*, 518–529.

Seidlitz, J., Váša, F., Shinn, M., Romero-Garcia, R., Whitaker, K.J., Vértes, P.E., Wagstyl, K., Kirkpatrick Reardon, P., Clasen, L., Liu, S., et al.; NSPN Consortium (2018). Morphometric similarity networks detect microscale cortical organization and predict inter-individual cognitive variation. Neuron *97*, 231–247.e7.

Seidlitz, J., Nadig, A., Liu, S., Bethlehem, R.A.I., Vértes, P.E., Morgan, S.E., Váša, F., Romero-Garcia, R., Lalonde, F.M., Clasen, L.S., et al. (2020). Transcriptomic and cellular decoding of regional brain vulnerability to neurogenetic disorders. Nat. Commun. *11*, 3358.

Smith, S.M., Jenkinson, M., Woolrich, M.W., Beckmann, C.F., Behrens, T.E., Johansen-Berg, H., Bannister, P.R., De Luca, M., Drobnjak, I., Flitney, D.E., et al. (2004). Advances in functional and structural MR image analysis and implementation as FSL. Neuroimage *23* (*Suppl 1*), S208–S219.

Thiebaut de Schotten, M., Urbanski, M., Batrancourt, B., Levy, R., Dubois, B., Cerliani, L., and Volle, E. (2017). Rostro-caudal architecture of the frontal lobes in humans. Cereb. Cortex *27*, 4033–4047.

Valk, S.L., Xu, T., Margulies, D.S., Masouleh, S.K., Paquola, C., Goulas, A., Kochunov, P., Smallwood, J., Yeo, B.T.T., Bernhardt, B.C., and Eickhoff, S.B. (2020). Shaping brain structure: Genetic and phylogenetic axes of macroscale organization of cortical thickness. Sci. Adv. *6*, eabb3417.

van den Heuvel, M.P., and Yeo, B.T.T. (2017). A spotlight on bridging microscale and macroscale human brain architecture. Neuron *93*, 1248–1251.

van den Heuvel, M.P., Kersbergen, K.J., de Reus, M.A., Keunen, K., Kahn, R.S., Groenendaal, F., de Vries, L.S., and Benders, M.J. (2015). The Neonatal Connectome During Preterm Brain Development. Cereb. Cortex *25*, 3000–3013.

Váša, F., Seidlitz, J., Romero-Garcia, R., Whitaker, K.J., Rosenthal, G., Vértes, P.E., Shinn, M., Alexander-Bloch, A., Fonagy, P., Dolan, R.J., et al.; NSPN consortium (2018). Adolescent tuning of association cortex in human structural brain networks. Cereb. Cortex *28*, 281–294.

Vázquez-Rodríguez, B., Suárez, L.E., Markello, R.D., Shafiei, G., Paquola, C., Hagmann, P., van den Heuvel, M.P., Bernhardt, B.C., Spreng, R.N., and Misic, B. (2019). Gradients of structure-function tethering across neocortex. Proc. Natl. Acad. Sci. USA *116*, 21219–21227.

von Economo, C.F., and Koskinas, G.N. (1925). Die Cytoarchitektonik der Hirnrinde des Erwachsenen Menschen. [The Cyto-Architectonics of the Cerebral Cortex of Adult Man.] (J. Springer).

Vos de Wael, R., Benkarim, O., Paquola, C., Lariviere, S., Royer, J., Tavakol, S., Xu, T., Hong, S.J., Langs, G., Valk, S., et al. (2020). BrainSpace: a toolbox for the analysis of macroscale gradients in neuroimaging and connectomics datasets. Commun. Biol. *3*, 103.

Wagstyl, K., Ronan, L., Goodyer, I.M., and Fletcher, P.C. (2015). Cortical thickness gradients in structural hierarchies. Neuroimage *111*, 241–250.

Wagstyl, K., Larocque, S., Cucurull, G., Lepage, C., Cohen, J.P., Bludau, S., Palomero-Gallagher, N., Lewis, L.B., Funck, T., Spitzer, H., et al. (2020). BigBrain 3D atlas of cortical layers: cortical and laminar thickness gradients diverge in sensory and motor cortices. PLoS Biol. *18*, e3000678.

Wang, R.A., Benner, T., Sorensen, A., and Wedeen, V.J. (2007). Diffusion Toolkit: a software package for diffusion imaging data processing and tractography. In Proceedings of the Joint Annual Meeting ISMRM-ESMRMB (ISMRM & SMRT), p. 3720.

Wei, Y., Scholtens, L.H., Turk, E., and van den Heuvel, M.P. (2018). Multiscale examination of cytoarchitectonic similarity and human brain connectivity. Netw. Neurosci. *3*, 124–137.

Yang, S., Meng, Y., Li, J., Li, B., Fan, Y.S., Chen, H., and Liao, W. (2020). The thalamic functional gradient and its relationship to structural basis and cognitive relevance. Neuroimage *218*, 116960.

Yarkoni, T., Poldrack, R.A., Nichols, T.E., Van Essen, D.C., and Wager, T.D. (2011). Large-scale automated synthesis of human functional neuroimaging data. Nat. Methods *8*, 665–670.

Zhang, J., Scholtens, L.H., Wei, Y., van den Heuvel, M.P., Chanes, L., and Barrett, L.F. (2020). Topography impacts topology: anatomically central areas exhibit a "high-level connector" profile in the human cortex. Cereb. Cortex *30*, 1357–1365.

Zilles, K., and Amunts, K. (2012). Neuroscience: segregation and wiring in the brain. Science *335*, 1582–1584.

Zilles, K., and Palomero-Gallagher, N. (2017). Multiple transmitter receptors in regions and layers of the human cerebral cortex. Front. Neuroanat. *11*, 78.

STAR★METHODS

KEY RESOURCES TABLE

REAGENT or RESOURCE	SOURCE	IDENTIFIER
Deposited data		
Processed neuroimage data from Jinling Hospital	This paper	https://figshare.com/articles/dataset/MS_Gradient/14977899
Code and data used	This paper	https://zenodo.org/record/5144162
Neuroimaging data from HCP	Human Connectome Project	https://db.humanconnectome.org/
Gene expression data from human brain	Allen Human Brain Atlas (AHBA)	http://human.brain-map.org
Histological atlas	BigBrain Project	https://bigbrain.loris.ca
T1w/T2w gradient and MPC gradient	(Paquola et al., 2019b)	https://github.com/MICA-MNI/micaopen/tree/master/MPC
Evolutionary expansion map	(Hill et al., 2010)	http://brainvis.wustl.edu/wiki/index.php/Sums:About
Software and algorithms		
FreeSurfer (v6.0)	(Fischl, 2012)	https://surfer.nmr.mgh.harvard.edu/
FSL (v5.0.9)	(Jenkinson et al., 2012)	https://fsl.fmrib.ox.ac.uk/fsl/fslwiki
MATLAB	N/A	
wb_view	Connectome Workbench	https://www.humanconnectome.org/software/get-connectome-workbench
BrainSpace toolbox	(Vos de Wael et al., 2020)	https://brainspace.readthedocs.io
Abagen toolbox	(Markello et al., 2021)	https://github.com/netneurolab/abagen
relaimpo R package (v.2.2.3)	(Grömping, 2006)	http://prof.beuth-hochschule.de/groemping/software/relaimpo/
NeuroSynth	(Yarkoni et al., 2011)	https://neurosynth.org/

RESOURCE AVAILABILITY

Lead contact

Further information and requests for resources should be directed to and will be fulfilled by the lead contact, Wei Liao (weiliao.wl@gmail.com).

Materials availability

This study did not generate new unique reagents.

Data and code availability

- Processed data have been deposited at Figshare, and are publicly available as of the date of publication. DOIs are listed in the Key resources table. This paper also analyzes existing, publicly available data. These accession numbers for the datasets are listed in the Key resources table.
- All original code has been deposited at Zendo and is publicly available as of the date of publication. DOIs are listed in the Key resources table.
- Any additional information required to reanalyze the data reported in this paper is available from the lead contact upon request.

EXPERIMENTAL MODEL AND SUBJECT DETAILS

This work included a sample of healthy adults (n = 119, mean age ± standard error of the mean (SEM) = 25.77 ± 0.61 years, 58 females) at Jinling Hospital, Nanjing University. This study was performed according to the Helsinki Declaration of 1975 and was approved by the local medical ethics committee at Jinling Hospital, School of Medicine, Nanjing University. Written informed consent was obtained from all subjects. All subjects had no history of neurological disorder or psychiatric illness and no gross abnormalities on brain MRI images.

METHOD DETAILS

Data acquisition

Multi-contrast MRI data were acquired using a Trio 3.0-Tesla MRI scanner (Siemens, Washington, DC, USA) at Jinling Hospital, Nanjing, China. Foam padding was used to minimize head motion. All subjects were required to keep their eyes closed and to keep their head still. The structural MRI (T1w) data were acquired in a sagittal orientation using a magnetization-prepared rapid gradient-echo sequence (repetition time (TR)/echo time (TE) = 2,300/2.98 ms, flip angle = 9°, field of view (FOV) = 256 × 256 mm^2, matrix size = 256 × 256, slice thickness = 1 mm, no interslice gap, and 176 slices).

Resting-state functional MRI (rs-fMRI) were acquired using an echo-planar imaging sequence (TR/TE = 2,000 ms/30 ms, flip angle = 90°). Thirty transverse slices (FOV = 240 × 240 mm^2, matrix size = 64 × 64, slice thickness = 4 mm, interslice gap = 0.4 mm) that aligned along the anterior commissure-posterior commissure line were acquired with a total of 250 volumes.

The diffusion weighted images (DWI) were obtained in parts of the subjects (n = 99) using spin an echo-based echo planar imaging sequence, including 30 volumes with diffusion gradients applied along 30 non-collinear directions (b = 1,000 s/mm^2) and one volume without diffusion weighting (b = 0 s/mm^2). Each volume consisted of 45 contiguous axial slices (TR/TE = 6,100 ms/93 ms, flip angle = 90, FOV = 240 × 240 mm^2, matrix size = 256 × 256).

MRI data preprocessing

Structural image processing pipeline was built using FreeSurfer version 6.0 software (https://surfer.nmr.mgh.harvard.edu/) (Fischl et al., 2001; Ségonne et al., 2007) and FSL (v5.0.9) (Jenkinson et al., 2002; Smith et al., 2004). Anatomical surfaces were generated from the individual T1w image in native space using the recon-all processing in FreeSurfer. Briefly, processing of the T1w image included skull stripping, cortical extraction and segmentation of cortical white and gray matter, separation of the hemispheres and subcortical structures (Fischl et al., 2004), and surface reconstruction of the gray/white interface and the pial surface.

Preprocessing of functional data included removing the first four frames, slice timing, motion correction using rigid body translation and rotation, and boundary-based registration to the T1w images (Greve and Fischl, 2009). The nuisance was then regressed, including the white matter, ventricular signal, global signal, six head motion parameters, and their temporal derivatives (Kong et al., 2019). The volume was defined as an outlier if the framewise displacement was > 0.5mm or the voxel-wise differentiated signal variance was > 50 when computed using FSL (Jenkinson et al., 2002; Smith et al., 2004). The data were interpolated across censored volumes, which was defined as i) one volume before and two volumes after these outliers, and ii) images are lasting fewer than five contiguous volumes (Gordon et al., 2016). Finally, the images were band-pass filtered (0.01–0.08 Hz). In the following exploratory analysis, three subjects were excluded due to non-ideal registration from the fMRI to T1w images.

The DWI images were corrected using a non-diffusion-weighted B0 image and a filed map for accounting for the eddy-current-induced distortions and reduced head movements. Diffusion tensor models were estimated using the Diffusion Toolkit by the least-squares fitting (Wang et al., 2007). Diffusion maps were registered to individual T1w images using FSL's (FLIRT) (https://fsl.fmrib.ox.ac.uk/fsl/fslwiki/). All functional and DWI images were visually inspected for motion artifacts and low quality of processed registration.

MS gradients analysis

The cortical surface was initially parcellated into spatially continuous and equal-sized cortical parcellations derived from the DK-68 atlas (Desikan et al., 2006). Considering that increased spatial resolution of the gradients became more pronounced (Vos de Wael et al., 2020), the size of each region was defined using approximately 1 cm^2, which resulted in 1,533 parcellations in the surface, referred to as the DK-1533 atlas (Romero-Garcia et al., 2012). This standard anatomical template was transformed to each subject's surface and was then interpolated to their volume space. Based on the individual surface and volume templates, five structural features were extracted from the individual's T1w data, including the GM, SA, CT, GC, and MC. Due to the lack of the DWI in some subjects (n = 20), and the non-ideal registration effect in other subjects (n = 21), the exploratory analyses were estimated using five morphometric features obtained from T1w data.

To characterize the topographic organization of MS connectomes, we performed diffusion map embedding (Margulies et al., 2016) to identify spatial axes of interareal structural variations. This nonlinear reduction technique allowed local and long-distance connections of the structural connectome to project into a common space. In this space, referred to as the "*gradient*", brain regions with more similar connections to others occupied similar positions. A set of gradients explaining spatial variations in the structural connectome were evaluated using the BrainSpace toolbox (Vos de Wael et al., 2020). According to previous studies (Hong et al., 2019; Margulies et al., 2016; Paquola et al., 2019b; Yang et al., 2020), we used the top 10% of connections per row to compute a cosine matrix which captured similarities in the profiles of structural connectomes. The manifold parameters followed recommendations and set $\alpha = 0.5$ and t = 0, which retained global relations between data points in the embedded space. After estimating the component template that was generated from the average MS matrix based on all subjects, each individual's MS gradient was aligned to this template. Finally, group-level MS gradients were generated across these aligned individual gradients. Evidence from nonhuman primates and human brains showed that anatomical connectivity is stronger between microstructurally similar areas than between cytoarchitecturally distinct areas (Barbas and Rempel-Clower, 1997; Wei et al., 2018). We, therefore, compared the anatomical distributions of the MS gradient within cytoarchitectural classes based on the Von Economo atlas (von Economo and Koskinas, 1925).

We next tested the different contributions of single cortical features to the stability of the MS gradient with the exclusion of one morphometric measure before MS connectome construction. To test the robustness of the MS gradient to the number of features and spatial resolution of cortical parcellations, we re-mapped the MS gradient with seven features (CT, GM, SA, GC, MC, FA, and ADC) to construct individual MS connectomes from the subjects who had an ideal registration of diffusion MRI to T1w images. These seven structural features were extracted from DK-308, with each of the parcels having a larger area, because some parcels would be missing from a smaller area when the diffusion MRI was registered to the T1 space.

Hierarchical organization analysis

To understand the hierarchical organization of the principal MS gradient, we investigated whether it was related to the intrinsic geometry of the cortex, a proxy of cortical hierarchical organization. We calculated the spatial correlation between the gradients and geodesic distance from primary areas in four local hierarchies, including the somatosensory, visual, auditory, and motor hierarchies. To do so, we selected the primary areas created from the labels in the Destrieux et al. (2010) atlas, including the calcarine sulcus, temporal transverse sulcus, and central sulcus, which demarcated the cortical landmarks of the primary cortex. For each primary cortex, a pre-defined large area containing associated cortical regions was identified based on the Brodmann atlas according to the sensory-fugal processing hierarchy proposed by Mesulam (1998) and a recent study (Wagstyl et al., 2020). To define the primary associated cortices in the DK-1533 atlas, we calculated the overlap of each parcellation in the DK-1533 with pre-defined areas. If more than half of the vertices in the parcellation were contained in the pre-defined area, this parcellation was identified into associated regions. The geodesic distance was measured as the shortest path across mid-surface between the vertex nearest to the centroid of each parcellation and the corresponding seed primary region (Oligschläger et al., 2017). A distance value was assigned to each parcellation based on the minimum distance to any of the seed parcellations (Margulies et al., 2016). We used the laminar histological atlas to understand the link between the MS gradient and mesoscale cortical layering and macroscopic cortical feature, which quantifies cortical and laminar thickness with high precision based on a 3D reconstructed BigBrain (Amunts et al., 2013; Wagstyl et al., 2020). We further performed a multiple linear regression model combining each of the six laminar atlases, and the dependent variable for the model was the MS gradient within each parcel. The relative importance of each laminar regression contribution to the bootstrapping regressor model was assessed using the *relaimpo* R package, v.2.2.3 (Grömping, 2006). Specifically, the relative contribution of each variable to the variation in the predicted MS gradient was assessed using the *pmvd* metric of the *relaimpo* R package.

Relation to cortical microstructure

To reveal the potential biological interpretation of the MS gradient in different biological scales, we analyzed its relation to the cortical microstructural profiles and evolutionary properties. First, we quantified the concordance between the MS gradient and systematic spatial variation of brain-wide gene expression. Parcel-wise microarray expression data were obtained from six post-mortem brains provided by the Allen Human Brain Atlas (AHBA; http://human.brain-map.org/) (Hawrylycz et al., 2012). We processed and mapped the data onto the DK-1533 atlas through the *abagen* toolbox (https://github.com/netneurolab/abagen). Briefly, probes were reannotated with information (Arnatkeviciute et al., 2019) and filtered with an intensity-based threshold of 0.5. After this procedure, 15,633 probes survived. Brain tissue samples were mirrored across the right and left hemispheres and then matched to parcels for each donor. For each parcel, samples assigned to the same area were separately averaged for each donor. Next, gene expressions were normalized across regions and finally averaged across donors to result in a matrix (1,533 regions × 15,632 gene expression levels). We used 1,899 brain-specific genes for the following analysis (https://github.com/weiliao81/MS-Gradient) (Burt et al., 2018). Principal component analysis was performed to identify the dominant spatial variation of brain-specific gene expressions in the human cortex. First, the spatial covariance matrix was constructed, and eigen decomposition was used to obtain the matrix principal components. We chose the first component, which captured variance in cortical gene expression profiles.

We then quantify the spatial concordance between the MS gradient and large-scale cytoarchitecture and myeloarchitecture of cortical organizations. One approach, known as microstructure profile covariance (MPC), described cortical interregional similarity in cortical microstructures (Paquola et al., 2019a, 2019b). The MPC gradients captured cellular density and myelin content changes in a cortical organization based on a 3D histological brain (BigBrain; https://bigbrain.loris.ca/main.php) (Amunts et al., 2013) and T1w/T2w MRI. These gradients delineated system-level spatial representations of microstructural similarity and captured a sensory-fugal gradient in cortical organizations. We download the MPC gradient maps (Paquola et al., 2019b) from https://github.com/MICA-MNI/micaopen/tree/master/MPC. Because the MPC gradient was constructed on a cortical surface with 1,012 spatial nodes of approximately 1.5 cm^2, we extracted the mean MPC gradient value within each region based on the DK-68 atlas to minimize the spatial bias. We then evaluated the spatial correspondence of the principal MS gradient to the cyto- and myeloarchitectural gradients. Moreover, to understand how evolutionary properties constrained the interregional morphological similarity, we also compared the MS gradient to maps of evolutionary cortical expansion. We download the evolutionary expansion map (Hill et al., 2010) from http://brainvis.wustl.edu/wiki/index.php/Sums:About.

Relation to functional gradients

To examine the role of the MS gradient in functional organizations, we compared the spatial correspondence of the cortical morphometric gradients to canonical functional gradients. To this end, we computed the individual functional connectivity (FC) matrix based

on the individual DK-1533 template, and the mean time series within each parcellation was extracted to construct the FC matrix by computing the pairwise Pearson's correlation coefficient. The top 10% of connectivity per row of the FC matrix remained to generate a cosine matrix. The individual FC gradients were generated using diffusion map embedding with the same parameters as the MS gradients. Each individual's gradient was aligned to the group template component, which was generated from an average functional connectivity matrix based on all subjects. Finally, a group-level FC gradient was mapped onto the DK-1533 atlas. We also assessed the relationships between the FC gradient and the geodesic distance from primary areas from the whole cortex and four local hierarchies.

To study topological features of the morphometric and functional gradients in hierarchical organizations, we directly calculated the differences in the MS and FC gradients by comparing region ranks across the whole cortex. To further localize the differences in the gradients, we compared node ranks within functional communities and cytoarchitectural classes. According to its underlying vertices, each parcellation in the DK-1533 atlas was assigned to one functional community/cytoarchitectural class. The MS and FC gradients were discretized into 50 equally sized bins. We calculated the proportion of each bin accounted for by each functional community/cytoarchitecture class and performed paired t tests to compare the region rank within the community/class between the MS and FC gradients across individuals. We also conducted a meta-analytical functional decoding analysis (Yang et al., 2020) using the Neurosynth database and examined the associations between nodes of interest created from 20 bins of the principal MS gradient with a list of terms that were similar to Margulies et al. (2016).

QUANTIFICATION AND STATISTICAL ANALYSIS

Reproducibility analysis

To evaluate the reproducibility of MS gradients, we repeated the gradient analyses across healthy control subjects in three independent datasets provided in the *Morgan* et al. study (Morgan et al., 2019). Details about the datasets have been previously published. We downloaded the morphometric features data from https://figshare.com/articles/Data_for_Cortical_patterning_of_abnormal_morphometric_similarity_in_psychosis_is_associated_with_brain_expression_of_schizophrenia-related_genes_/7908488/1. We also studied data from 339 unrelated healthy adults from the minimally preprocessed S900 release of the HCP (https://wiki.humanconnectome.org/display/PublicData/S900+Unrelated+Subjects+CSV) and extracted five cortical features to construct the MS gradient map. We estimated the spatial correlation of the principal MS gradient from the exploratory data and retested data. The HCP data were acquired using protocols approved by the Washington University institutional review board and shared on the ConnectomeDB database (Hodge et al., 2016). Full details for the HCP dataset have been previously published (Glasser et al., 2013).

Statistical analysis

In the current study, measures were related to each other across parcels. Spatial correspondences analyses were estimated via Spearman's correlation with 1,000 spin test permutations to control spatial autocorrelations (Alexander-Bloch et al., 2018; Váša et al., 2018). The spin test generated a set of null correlations by randomly rotating the spherical projection of the spatial maps. Thus, each correlating analysis is reported with the empirical Spearman's Rho and the spherical permutation P_{spin}. We performed paired t tests to compare the region rank within the community/class between the MS and FC gradients across individuals. The statistical outcome of paired t tests were listed in Table S2.